Ore Geology Reviews 74 (2016) 76–87

Contents lists available at ScienceDirect

Ore Geology Reviews

journal homepage: www.elsevier.com/locate/oregeorev

New ASTER derived thermal indices to delineate mineralogy of different granitoids of an Archaean Craton and analysis of their potentials with reference to Ninomiya's indices for delineating quartz and mafic minerals of granitoids—An analysis in Dharwar Craton, India

Arindam Guha *, Vinod Kumar K.

Geosciences Group, National Remote Sensing Centre, Indian Space Research Organisation, Balanagar, Hyderabad, India

ARTICLE INFO

Article history:
Received 31 July 2015
Received in revised form 27 October 2015
Accepted 31 October 2015
Available online 2 November 2015

Keywords:
ASTER
Thermal bands
Emissivity normalisation method
granitoids
FRI
QRI
MRI
Ninomiya's quartz and mafic indices

ABSTRACT

We processed five thermal infrared (TIR) bands of Advanced Spaceborne Thermal Emission and Reflection Radiometer (ASTER) "at-sensor radiance" (Level 1B) data to derive few new indices to delineate variation in quartz, feldspar and mafic minerals in three different variants of granitoid; commonly occurring quartz bearing intrusive rock group. In this regard, three indices named as quartz-bearing rock index (QRI), feldspar-bearing rock index (FRI) and mafic-bearing rock index(MRI) were proposed.QRI index was derived using band 10, band 12 and band 13((band 10/band 12) * (band 13/band 12)) of ASTER radiance image. MRI index was derived using band 12, band 13 and band 14 ((band 12/band 13) * (band 13/band 14)) of ASTER radiance bands while band 10, band 11 were combined to derive FRI ((band 10/band 11) index. Three indices were combined in false colour composite image (FCC) and three-dimensional scatter plot to delineate granite, alkali granite and mafic rich granodioritic gneiss from each other as these granitoids had variable abundances of quartz, feldspar and mafic minerals. QRI and MRI were compared with the corresponding quartz and mafic indices proposed by Ninomiya (2005). It was observed from the respective ratio images and their regression plots that MRI and Ninomiya's mafic index (NMI) were complementary to each other. On the other hand, QRI image was better in enhancing quartz enrichment in alkali granites than Ninomiya's quartz index (NQI).However, QRI index was comparable with the quartz index proposed by Rockwall and Hofstra (2008) in terms of delineating quartz enrichment in alkali granite. Mutual exclusive nature of mafic minerals and quartz in granitoids was also evident from the negative correlation between MRI and QRI indices of the granitoids. On the other hand, FRI and QRI were negatively correlated with low regression value. This was resulted due to the combined effect of inverse relation of abundance of two dominant feldspars with quartz in different granitoids. In granitoids, abundance of plagioclase is known to increase with decreasing quartz content in granodiorite and tonalite although alkali feldspar bearing granites are characterised with high silica content. Results of discrimination of granitoids using proposed indices were validated based on deriving emissivity spectra of rocks and comparing them with ASTER TIR band resampled laboratory spectra of respective granitoids in addition to use geological map of the study area. Emissivity spectra of granitoids were derived from emissivity image (derived using emissivity normalisation method) after geospatially tagging it with QRI–FRI–MRI image composite; which was used to delineate exposures of granitoids. Further, we also found that the QRI, MRI and FRI indices had poor temperature dependence; when these indices were compared with relative surface temperature image derived from radiance bands using emissivity normalisation algorithm. Therefore, proposed indices can be implemented for delineating mineralogical variations of granitoids irrespective of surface temperature condition. Hence, proposed indices may be used successfully to delineate different granitic intrusions and relating their mineralogical variations with metallogeny.

1. Introduction

The important rock-forming minerals such as quartz and feldspar are not characterised with absorption features in their reflectance spectra collected within the spectral domain of the visible-near-infrared (VNIR) and short wave infrared (SWIR) regions (as it was the case

* Corresponding author.
E-mail addresses: arindamisro@gmail.com (A. Guha), vinodkumar_k@nrsc.gov.in (V.K. K.).

http://dx.doi.org/10.1016/j.oregeorev.2015.10.033
0169-1368/

for clay minerals, oxides–hydroxides, carbonates etc.) (Lyon, 1972; Salisbury and Walter, 1989). On the other hand, thermal infrared (TIR) region is extremely useful for the spectral discrimination of these minerals based on differences in the emissivity spectra resulted due to variable vibration modes of Si–O bonds of major rock forming silicate minerals (Farmer, 1974; Kahle, 1976; Lyon, 1972).The subtle differences in the bonding of silicates are responsible for shifting of the emissivity minima in the TIR spectra of silicate bearing rocks (Salisbury and Walter, 1989; Salisbury and D'Aria, 1992).Geological mapping is an integral part in many of the geoscientific disciplines like mineral exploration, geo-environment and geo-engineering sciences. In conventional geological mapping, rock types are delineated by integrated analysis of qualitative and quantitative field data with mineralogical data on rock exposures. Mineralogical data are derived from X-ray diffraction (XRD) analysis and petrographical studies of optical thin sections of rock samples. Field data and mineralogical data are also often combined with geochemical data on elemental abundance to delineate intra or inter-rock compositional changes. In this regard, spectroscopic data are often used to identify the minerals present in the rocks of the earth's surface and also in the other planets based on identification of absorption features in the spectral profiles of rocks and minerals. These spectral features are collected within wider wavelength range encompassing VNIR (04.1.0 μm), SWIR (1.0–2.5 μm), mid-infrared (MIR) (3–5 μm) and TIR (8–14 μm) electromagnetic domains. Mineralogical dependence of TIR spectroscopy especially, its sensitiveness to silicate structures provides scope for mapping different rock types based on thermal characters of constituent minerals. This is particularly useful for geological mapping and classification of primary rocks, i.e. igneous rocks and also selected metamorphic rocks; which are rich in recrystallised silicate and carbonate minerals. Most rock forming minerals like silicates and carbonates exhibit diagnostic emissivity features in the TIR region. But TIR emissivity spectra are less studied and utilised for spatial delineation of natural targets like rocks in comparison to VNIR–SWIR reflectance spectra. This is due to the fact that very few hyperspectral (spectral observation in contiguous channels) and multispectral space-borne sensors are operative in TIR domain. It is in turn related to poor signal-to-noise (SNR) of data recorded by the thermal channels within TIR domain (Gillespie, 1985). This is another hindrance for using contiguous spectral bands with finer spectral resolution to detect subtle variation in thermal emissivity within the TIR wavelength range.

Advanced Spaceborne Thermal Emission and Reflection Radiometer (ASTER) launched on board the EOS-Terra satellite, is a multi-spectral sensor system (Abrams, 2000). ASTER has three bands in VNIR domain, six bands in short wave infrared SWIR domain and five bands (band numbers 10 to 12) in TIR domain. ASTER data have been extensively used for mapping few significant types of surface mineralisation signatures associated with hydrothermal alteration zones and oxidation capping of supergene enrichment deposit based on the diagnostic absorption features of different clay, carbonate, aluminium-iron hydroxide minerals in VNIR–SWIR domain (Abrams, 2000; van der Meer et al., 2012; Zhang et al., 2007)). Further VNIR–SWIR bands of ASTER were also used for delineating few economic rock types constituted with spectrally sensitive minerals (Abrams, 2000; Guha et al., 2013a,b, 2014; Rajendran et al., 2011a; van der Meer et al., 2012).

In recent times, different thermal false colour composites and thermal band ratio images have been used to delineate rock types (Ding et al., 2014; Gomez et al., 2005; Kalinowski and Oliver, 2004; Matar and Bamousa, 2013; Ninomiya et al., 2005; Rajendran and Nasir, 2014). It is observed that quartzo-feldspathic rocks like granite and silica rich dry river sand appear with reddish colour in the L1B daytime (geo-rectified "at-sensor radiance" data) false colour composite image derived using red, green and blue colour assignment to band 14, band 12 and band 10 of ASTER sensor respectively (Yajima and Yamaguchi, 2013). This is due to the fact that the spectral emissivity of quartz is relatively lower in the 8–9 μm region (band 10 to band 12 of ASTER TIR sensor) than in the 10–12 μm region (band 13 and band 14 of ASTER TIR sensor). Feldspar also has emissivity minima in band 11 of ASTER sensor. But mafic rocks appear white or bright grey in TIR false colour image prepared using band 12, band 11 and band 10 (first three bands) of ASTER thermal sensor in red- green- blue (RGB) colour space as mafic minerals have relatively higher (in comparison to quartz and feldspar) and similar spectral emissivities in 8–9 μm region (Yajima and Yamaguchi, 2013).Based on analysis of ASTER TIR band based emissivity spectra of rocks, Ninomiya et al. (2005) have proposed few popular spectral indices for the mapping of quartz, carbonate, and mafic rocks using ASTER data. Many important geological units were also mapped using TIR bands of ASTER data using emissivity as a parameter (Bertoldi et al., 2011; Ding et al., 2014; Matar and Bamousa, 2013; Ninomiya et al., 1997, 2005; Rowan et al., 2005). But derivation of multi-channel thermal emissivity from space-borne data is a challenge as contrast in spectral emissivity collected in few thermal bands (operative within specified spectral domain) is very less for commonly occurring terrain elements. Striping noise was also reported in emissivity bands derived from ASTER level 1B data due to poor SNR in multiband emissivity data (Son et al., 2014). However, mineralogically sensitive indices often derived significant results in terms of delineating mineralogical contrast by highlighting variations in thermal emissivity of terrain elements recorded in selected numbers of bands. Utilization of ASTER TIR bands for mapping of different granitoids of Archaean Dharwar Craton is a challenge as each granitoid variant represents specific mineralogy and specific stage of magmatic differentiation of parent magma. The term granitoids include family of felsic igneous rocks viz. alkali granites, granites, granodiorites, tonalities; which are essentially constituted with quartz, varied proportions of alkali feldspar and plagioclase feldspar (Bose, 1997). Alkali feldspar rich granite is characterised with high ratio of alkali feldspar to plagioclase feldspar content whereas the ratio is progressively lower in granodiorite and tonalite (Bose, 1997). Mafic mineral content (biotite, hornblende etc.) is low in granitoids in general. However, mafic mineral abundances are also progressively higher as we go from granite to tonalite in granite–granodiorite–tonalite sequence.

Each granitoid province of Archaean and Proterozoic terrain is known for the presence of different granitoids each of which has specific range of mafic mineral and quartz content. Alkali feldspar to plagioclase feldspar abundance ratio is also distinct in each variant. It is important to enhance some of these mineralogical variations of granitoid using ASTER thermal bands. Delineation of different sub variants of granitoids with varying quartz and alkali feldspar content would provide Precambrian geologists a scope to identify the relative stage of differentiation involved in the evolution of granitoids. This would also help in understanding the different chronological events of granite emplacement and how these granitoids are related to Archaean greenstone rocks (i.e. either intrusive or basement).

In the present study, we have attempted to identify different granitoids by delineating variations in quartz, mafic and feldspar content in these rocks using thermal bands of space borne ASTER sensor. In this regard, we have processed ASTER "at-sensor radiance" thermal bands to delineate mineralogical contrast of granitoids based on derivation of few indices; which are effective in delineating broad mineralogical variations of key minerals like quartz, feldspar and mafic minerals. Multistage enhancements of thermal spectral features based on derivation of indices to understand mineralogical variations of quartz, feldspar and mafic minerals proved important in identifying granitoids and also in sub-categorising them (Ding et al., 2015).

In this regard, researchers also have concluded based on their study that the indices directly derived from ASTER Level-1B radiance data would be more effective and accurate than the indices derived from emissivity image for detection of specific minerals and rocks (Ding et al., 2014). One advantage of using Level 1B data is that lower-level data (i.e. level 1B) are free of functional uncertainties introduced by the atmospheric-correction methods and temperature separation algorithms on spectral emissivity (Ninomiya et al., 2005; Ding et al., 2015). Researchers have demonstrated the utility of ASTER level 1B data in derivation of mineralogically sensitive indices (Chen and Wang, 2007;

Ninomiya et al., 2005; Rajendran et al., 2011b; Matar and Bamousa, 2013; Aboelkhair et al., 2010; Ding et al., 2014, 2015). The results of these studies were considered seriously to select the type of ASTER data to meet the objective of the present work. Hence, we have selected level 1B data for meeting our research objectives.

The results of index images are analysed using a geological map of the study area of Geological Survey of India (in 1:250,000 scale). New indices are also compared with similar established indices with respect to delineation of different sub-variants of granitoids. Mineralogical importance of indices is also analysed with respect to known mineralogical framework of rocks of granite family. We further have validated results of indices based on comparison of ASTER TIR band derived emissivity spectra of selected variants of granitoid exposures of index composite image with ASTER TIR-band resampled laboratory spectra of respective rocks. In this regard, different granitoids delineated in index composite and emissivity image are geospatially linked with index composite image to collect the spectra of respective granitoid exposures from emissivity image.

Space-based study of delineation of different granitoids has ore genetic significance. Many important mineral deposits are either hosted by granite or formed from hydrothermal fluid associated with granite (tin, molybdenum, tungsten, lead-zinc, porphyry copper, rare earth, gold and sliver etc.). Ore systems associated with granites have been regarded as one of the important targets of the mineral exploration (Sial et al., 2011). A recent study on processing of thermal bands to delineate granitoid has also pointed out the importance of granitoids for exploring non-ferrous, rare earth and radioactive minerals (Ding et al., 2015).

2. Study area and geology

The study area is situated in the west and north-west part of Ananthpur district, Andhra Pradesh; well accessible by road from Ananthpur town. Ananthpur is situated in south-west of Hyderabad, one of the major cities of south India (Fig. 1.).The rocks of the study area are mainly Archaean–Proterozoic granitoids associated with metasediments/metavolcanics of Dharwar Super Group (Murthy and Ramam, 1997). "Granitoid" is a general term used to describe quartz-bearing felsic igneous rocks. Each of the sub-variants of granitoids has variable content of quartz, mafic and feldspar minerals (with different proportions of alkali and plagioclase feldspar). Main granitoids of the area (in terms of spatial extent) are Dharwar granodiorite gneiss. This rock is mainly exposed in the eastern part of the study area. The granodiorite gneiss is hornblende and biotite rich. The rock is weathered and covered with thick soil cover. In addition to this rock, orthoclase feldspar bearing Closepet granite is also exposed in the central and south-western part of the area. This rock is also known as pink granite due to prevalence of pink coloured orthoclase feldspar in this granite. (Fig. 1).Within these pink granites, few patches of pure granite exposures with low feldspar content than pink granite but with the same quartz content or slightly higher than alkali granite can be delineated. Geological map prepared by the Geological Survey of India at 1:250,000 scale is used as reference for interpreting the geological information derived from ASTER thermal bands with 90 m spatial resolution and 12 bit radiometric resolution.

3. Materials and methods

Broad methodology adopted to delineate different variants of granitoids using three new indices and comparative evaluation of two new indices with Ninomiya's indices has been illustrated in Fig. 2. Specification of ASTER thermal bands used in this study has been provided in Table 1. Earlier, ASTER level 1B data (at-sensor radiance) were successfully used to delineate mineralogical contrast based on derivation of ASTER thermal indices (Ninomiya et al., 2005). ASTER level 1B data were widely used in deriving mineralogical indices in thermal infrared domain (Ninomiya et al., 2005; Rajendran et al., 2011a,b; Matar and

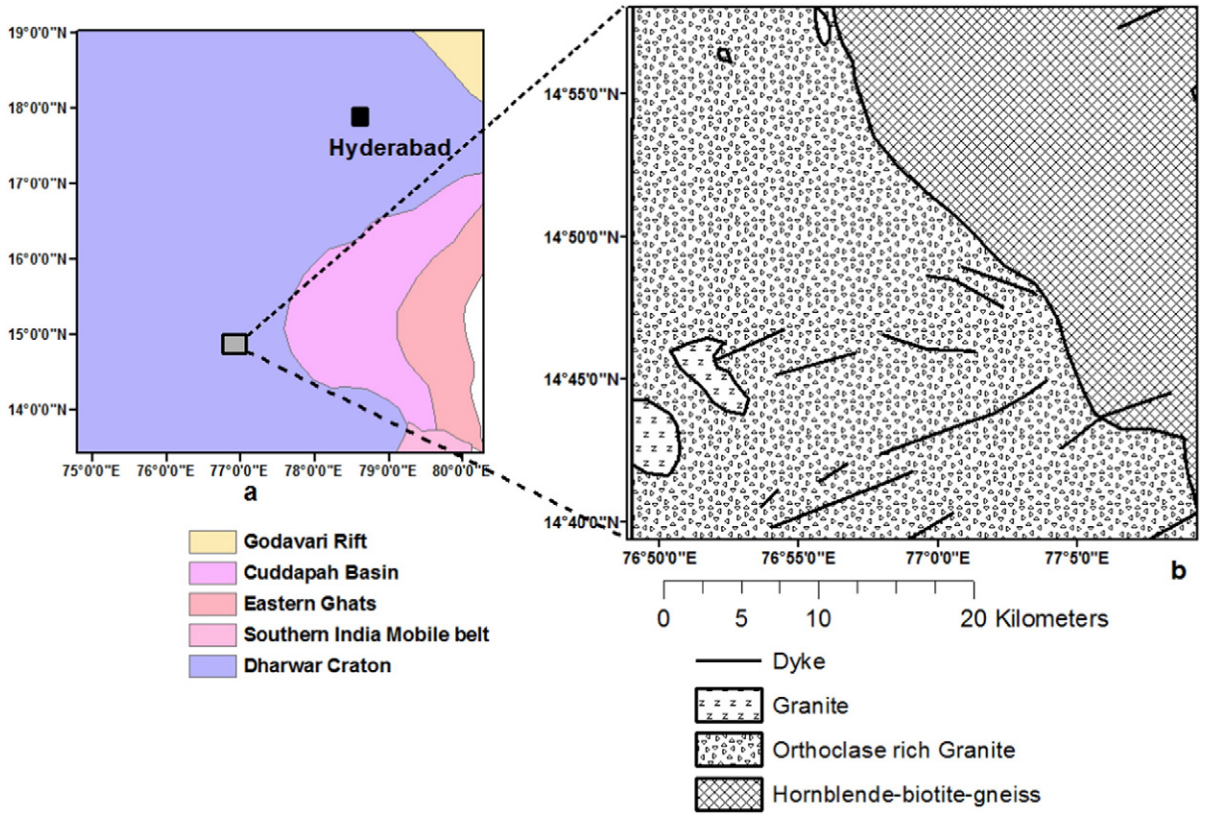

Fig. 1. a. Study area shown within regional geological set up of southern India (Modified after Drury et al., 1984). b. Geological map of the study area showing major litho units (reference map: District resource map of Ananthapur District, Andhra Pradesh. Geological Survey of India (1:250,000).

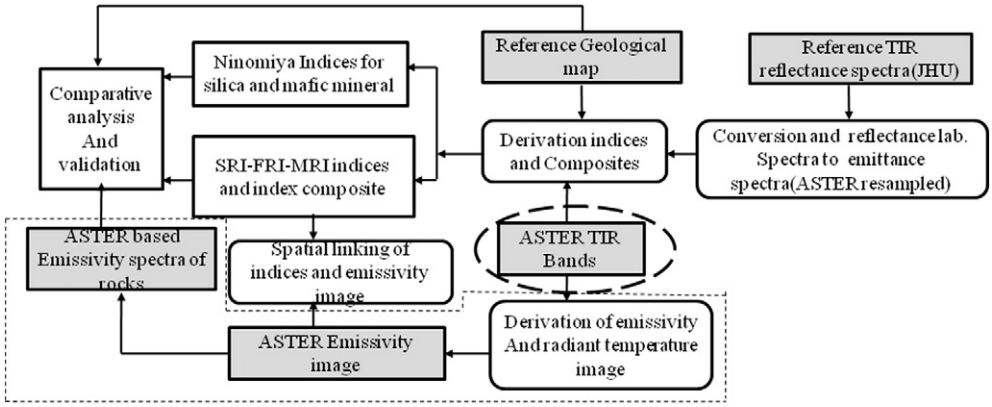

Fig. 2. Schematic diagram highlighting the work flow of methodology followed for processing ASTER thermal bands. (Portion shown within dotted line has been used as reference to validate the results obtained using indices to delineate granitoids).

Bamousa, 2013; Aboelkhair et al., 2010; Ding et al., 2014, 2015). Therefore, we used level 1B "at sensor- radiance" data to delineate few new indices comparable with Ninomiya's indices (for quartz and mafic minerals) without attempting any atmospheric correction to reduce the effect of those algorithms on original radiance signature. Different granitoids are known for low contrast in terms of thermal inertia (Gupta, 2003). Therefore, radiance contrast recorded in ASTER level 1B data was assumed to be primarily controlled by emissivity contrast. Emissivity patterns of these rocks were analysed based on evaluating ASTER thermal band resampled laboratory emissivity spectra of key constituent minerals of granitoids (Fig. 3). These emissivity spectra were normalised with respect to continuum to enhance the diagnostic emissivity minima of constituent minerals of granitoids as these emissivity minima were considered important for derivation of indices. Continuum is an imaginary line tangent to the emissivity spectra connecting background emissivity value points. Potentials of continuum in enhancing diagnostic spectral and emissivity signatures of mineral or rock spectra have been discussed in literatures (Okada and Iwashita, 1992; van der Meer et al., 2006). It is also known that the diagnostic spectral features of rocks and minerals are guided by constituent minerals and wavelength of absorption was regarded as the most consistent spectral parameter (Clark, 2011; Guha et al., 2012). We analysed resampled (i.e. resampled to the band width of ASTER thermal bands) laboratory derived emissivity spectra of quartz, orthoclase and plagioclase minerals; three key minerals of granitoids. It was observed that quartz was characterised with emissivity minima at band 12 (for quartz) with relative high in emissivity in band 10 and band 13 of ASTER bands. Feldspar is characterised with lower emissivity (for both plagioclase and orthoclase feldspar but the emissivity minima were more intense for orthoclase feldspar or K-feldspar) in band 11 than band 10 of ASTER thermal bands (Fig. 3). It is also known that mafic minerals and rocks are known for their emissivity minima in band 13 of ASTER sensor than band 12 and band 14 (Son et al., 2014). It was observed that emissivity spectra of quartz and feldspar had a reverse trend in band 11 and band 12 (Son et al., 2014). Therefore, emissivity minima of feldspar would be nullified by high emissivity of quartz in band 11 with respect to band 12 if quartz and feldspar are present in the same rock. Based on the above observations on emissivity spectra of constituent minerals of granitoids and their respective image spectra, the following indices were derived to delineate quartz, feldspar and mafic mineral variation in granitoids based on processing of ASTER bands.

$$\text{Quartz bearing rock index(QRI)} = (\text{band } 10/\text{band } 12) * (\text{band } 13/\text{band } 12)$$

$$\text{Mafic mineral bearing rock index(MRI)} = (\text{band } 12/\text{band } 13) * (\text{band } 14/\text{band } 13)$$

$$\text{Feldspar bearing rock index(FRI)} = (\text{band } 10/\text{band } 11) * (\text{band } 12/\text{band } 11)$$

QRI index was used to delineate high silica (quartz) bearing rocks. MRI was used to delineate granitoids based on mafic mineral variations. FRI was used to delineate rocks with high values of feldspar/quartz ratio. However, FRI would not be suitable to delineate the variation in orthoclase feldspar and plagioclase feldspar content in granitoid as two feldspars have their emissivity minima in band 11. In addition to the above indices, two indices one for quartz and another one for mafic minerals as proposed by Ninomiya et al. (2005) were derived. Another popular quartz index proposed by Rockwall and Hofstra (2008) was also derived. This index was originally proposed in ASTER Level-2 data. However, this index was derived from ASTER level 1B data here and also proved suitable to enhance silica enrichment in granite and alkali granite. In earlier studies, it was observed that this particular index was proved suitable to delineate quartz enrichment with lesser noise than Ninomiya's quartz index (Yajima, 2014). Mathematical expression of these established indices are outlined below.

$$\text{Ninomiya's quartz index(NQI)} : (\text{band } 11 * \text{band } 11/(\text{band } 10 * \text{band } 12)$$

$$\text{Ninomiya's proposed mafic index(NMI)} : \text{band } 12/\text{band } 13$$

$$\text{Quartz index proposed by Rockwall and Hofstra, } 2008\,(\text{QI}-\text{RH}) := (\text{band } 11/(\text{band } 10 + \text{band } 12)) * (\text{band } 13/\text{band } 12)$$

We evaluated the proposed indices for quartz(QRI) and mafic minerals(MRI) with respect to corresponding Ninomiya indices (NQI and NMI) based on comparison of the results obtained by implementing new and Ninomiya's index images to delineate different variants of granitoids in the study area. We also tested the performance of the

Table 1
Specification of ASTER data.

ASTER granule ID	Sensor type	ASTER band number	Spectral width (micrometer)	Spatial resolution(in metres)	Radiometric resolution
ASTL1A 090111053446090114020 0 (Date 14-01-2009)	TIR	10	8.125–8.475	90	12 bits
		11	8.8475–8.825	90	12 bits
		12	8.925–9.275	90	12 bits
		13	10.25–10.95	90	12 bits
		14	10.95–11.65	90	12 bits

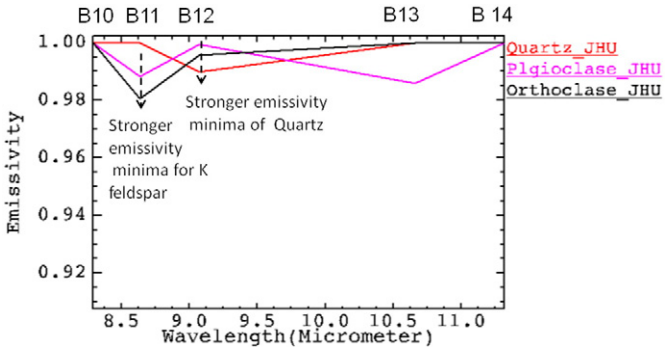

Fig. 3. ASTER TIR band resampled laboratory emissivity profiles (collected from JHU spectral library) of three major minerals of granitoids (quartz, alkali feldspar, plagioclase feldspar. Wavelength position of ASTER thermal bands are schematically shown on the plot.

proposed QRI index with respect to the performance of QI–RH. Further temperature dependences of these indices were also analysed using regression analysis of each index image with relative surface temperature image. This was derived while separating emissivity and temperature from radiance data using emissivity normalisation method (discussed in the next paragraph).

In order to cross-check the mineralogical information derived from proposed indices, we used image derived emissivity spectra of exposures of two selected variants of granitoids. These exposures were well identified in index-derived false colour composite (I-FCC). The emissivity spectra of two granitoid variants were derived from relative emissivity image; which was in turn deduced from ASTER level 1B bands using emissivity normalisation method. Potential of emissivity normalisation method in deriving characteristic spectral shape of terrain elements has been discussed in literature (Hook et al., 1992, 1999; Kealy and Hook, 1993; Li et al., 1999, 2013a,b; Peres and DaCamara, 2004; Guha and Vinod Kumar, 2014; ITT, 2014).Potential geological utility of relative emissivity and pixel temperature derived using emissivity normalisation method has also been discussed in literature (Guha and Vinod Kumar, in press).

The routine of ENVI 4.8 image processing software was used to derive emissivity from ASTER radiance bands. Emissivity and temperature of surface elements control the at-sensor radiance of space-borne thermal bands. Emissivity was therefore derived in two steps. In the first step of this method, temperature was derived for each band using fixed emissivity of 0.96 for each band (Li et al., 2013b; Guha and Vinod Kumar, 2014). This value was regarded as reasonable approximation of mean emissivity of terrain elements. The highest temperature derived for each pixel from such set of temperature values (each for a thermal band) was used to derive emissivity of each pixel for each thermal band using Planck's equation (Hook et al., 1999; Guha and Vinod Kumar, 2014; ITT, 2014). It was observed that the emissivity normalisation (NEM) method was more effective in delineating different terrain elements based on emissivity contrast in comparison to other emissivity extraction methods such as alpha residual and reference channel method while processing ASTER thermal bands(Li et al., 1999; Guha and Vinod Kumar, 2014). This method was identified as one of the best method for preserving the shape of broad band emissivity curve of terrain elements; which are related to mineralogical variations (Li et al., 1999). Further, it was also reported that the retrieved accuracy with NEM was consistent with derived accuracy of ASTER temperature

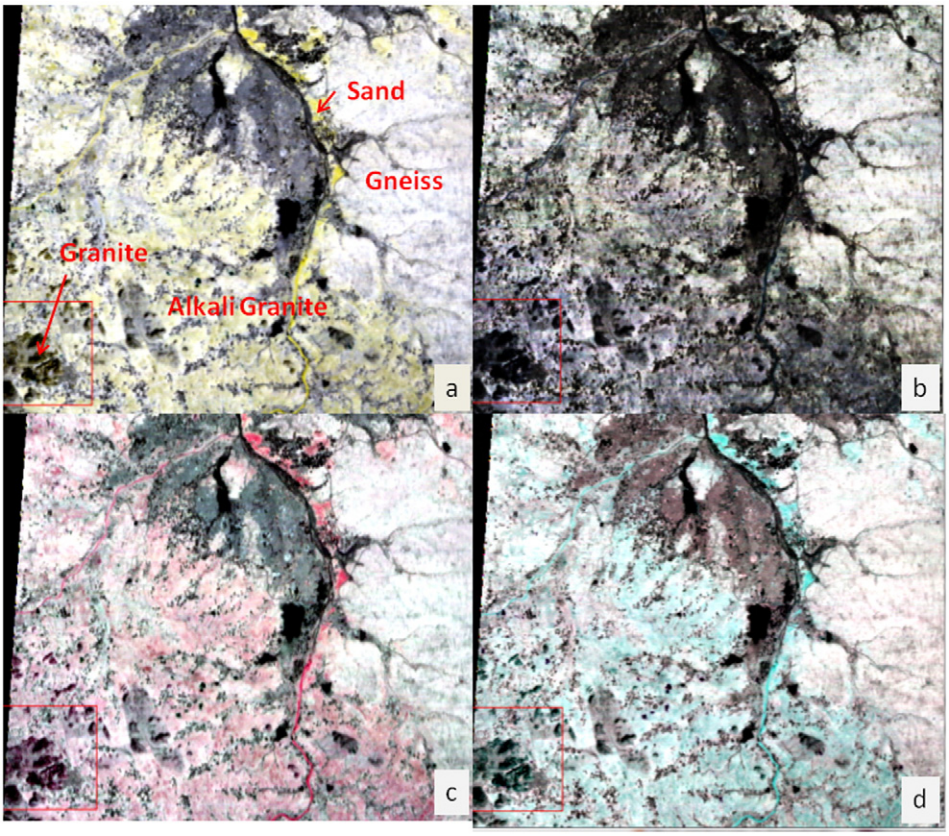

Fig. 4. a. ASTER thermal infrared (TIR) radiance composite.(Red = band 14, Green = band 13, Blue = band 12) of ASTER thermal radiance image. b ASTER thermal infrared (TIR) radiance composite.(Red = band 12, Green = band 11, Blue = band 10) of ASTER thermal radiance image. c. ASTER thermal infrared (TIR) radiance composite.(Red = band 14, Green = band 12, Blue = band 10) of ASTER thermal radiance image. d. ASTER thermal infrared(TIR) radiance composite.(Red = band 11, Green = band 14, Blue = band 13) of ASTER thermal radiance image.

emissivity separation (TES) method (Li et al., 2013b).Multi-band emissivity images derived from ASTER level 1B data using relative emissivity methods similar above had also shown potential in delineating different rock types (Nair and Mathew, 2012; Guha and Vinod Kumar, 2014).

As indicated above, the emissivity spectra of granitoids collected from emissivity image were used to validate the results of index composites in terms of delineating different granitoids. This was achieved by geospatially linking the exposures of granitoids from index composite image with corresponding image signatures in emissivity image to collect the emissivity spectra of selected variants of granites. These spectra were further compared with ASTER resampled laboratory spectra of corresponding granitoids.

4. Results

We found that quartz and feldspar minerals were characterised with contrasting spectral behaviour as observed from the ASTER resampled laboratory derived emissivity spectra (continuum removed) of these minerals especially in bands 11 and 12 of ASTER thermal sensor (Fig. 3). Emissivity minima were observed in band 12 for quartz whereas feldspar (K-rich and plagioclase rich feldspar both) had relatively

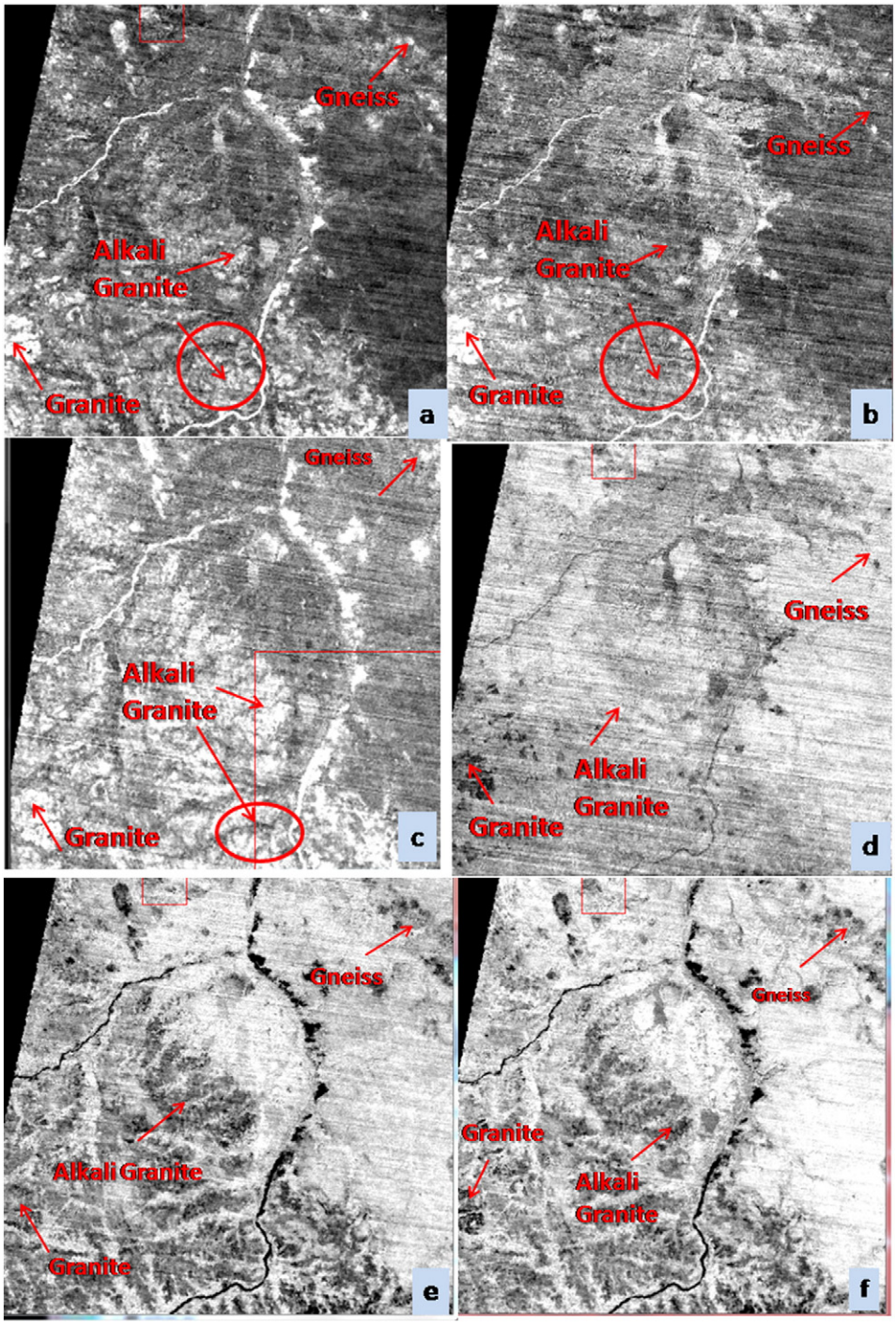

Fig. 5. a = Quartz-bearing rock Index (QRI) image. b. Ninomiya's quartz index (NQI) image. c = Rockwall and Hofstra index (2008)(QI–RH), d = Feldspar bearing rock index (FRI) image. e = Mafic-bearing rock index (MRI)image and = Ninomiya's mafic Index(NMI) image.

higher emittance in this band. On the other hand, higher emittance of quartz at band 11 of ASTER was nullified by emissivity minima for feldspar in the same band. Therefore, delineation of different granitoids; which are both quartz and feldspar rich is a tricky issue using these bands (bands 11 and 12). In this work, attempt has been made to derive three indices to delineate variation of three mineral groups' viz. quartz, feldspar and mafic minerals to subcategorise granitoids. The study area is dominantly made up of felsic rocks. We prepared different false colour composites (FCC) using ASTER thermal bands to delineate broad mineralogical contrast of these rocks. It was found that relatively quartz rich alkali granite and granite were delineated in these false colour composites from mafic rich and quartz deficient granodioritic–tonalitic gneiss based on colour contrast (Fig. 4.a.b.c.d). Granodiorite-tonalite-gneiss is also more weathered with its soil cover than other two granitoid variants (i.e. alkali granite and granite). Radiance FCC image prepared using band 14, band 12 and band 10 of ASTER sensor (Fig. 4) was characterised with red tint in most of part of the area (for silica rich alkali granite and granite) except soil covered portion of gneiss; which was colourless (Yajima and Yamaguchi, 2013). However, contrast between alkali granite and granite having different alkali feldspar content was poor in these radiance FCC composites although pure granitic patches are present within alkali granite country. This was confirmed by analysing these images using updated reference geological map (south western part of the study area) (Fig. 4.a and b). Therefore, we attempted to derive three new indices to delineate variation in quartz, feldspar and mafic mineral content in granitoids exposed in the study area (Fig. 5.a.d.e.). In general, different sub-categories of granitoids were identified based on variation in the content of three major mineral groups—quartz, feldspar (alkali-feldspar or plagioclase feldspar), mafic minerals (hornblende and biotite etc.) (Bose, 1997).Therefore, derivation of mineralogical indices of these minerals was essential to subcategorise silicate rocks like granitoids using ASTER thermal bands. We also derived quartz and mafic indices as proposed by earlier workers (Ninomiya et al., 2005). Ninomiya's quartz index (abbreviated as NQI in this study) and Ninomiya's mafic index (abbreviated as NMI in this study) were popularly used in earlier studies to find quartz and

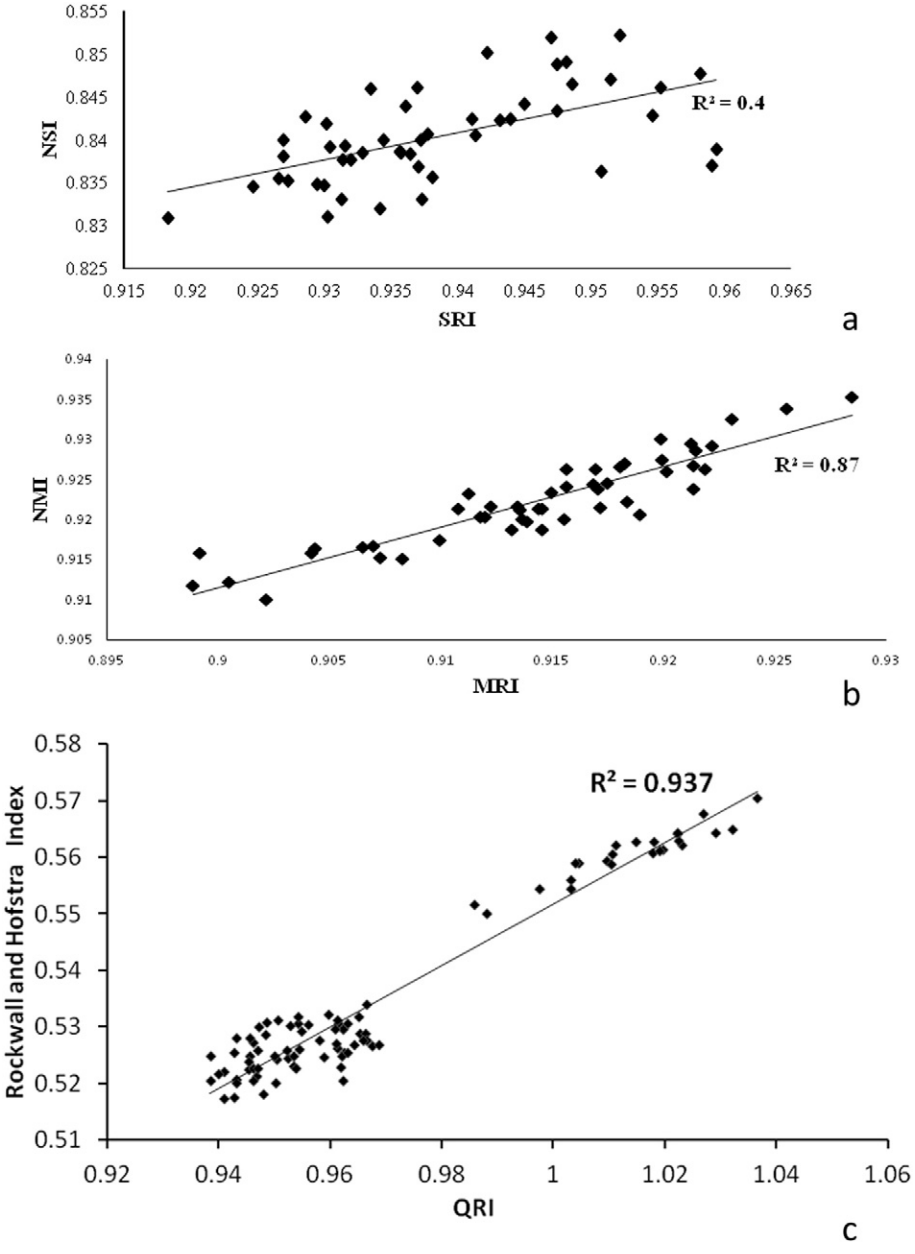

Fig. 6. a. Correlation between QRI and Ninomiya's quartz index. b. Correlation between MRI and Ninomiya's quartz index. c Correlation between SRI and Rockwall and Hofstra's Quartz index (2008).

mafic mineral variations in different terrain elements. But it was observed that silica variation in alkali-granite and granite was better enhanced in the proposed QRI image than NQI image (5.a and b). Quartz rich alkali granite appeared relatively darker in NQI image while the proposed QRI image could delineate quartz enrichment in this alkali-granite; which is relatively brighter in QRI index image. Conjugate use of band 11 and band 12 in NQI was the main issue for non-detection of quartz enrichment in alkali granite as it was done in QRI image. This is due to the fact quartz and feldspar are characterised with contrasting emissivity features in these bands. Therefore, it was difficult to delineate quartz enrichment in rocks which were rich in feldspar and quartz using band 11 and band 12. However, sandy river channels were bright in both QRI image and NQI image (Fig. 5.a and b). We also compared the results of the proposed QRI image with quartz index image proposed by Rockwall and Hofstra (2008). In this index (QI–RH); it was assumed that emittance would be higher in band 11 for quartz as it was proposed by Ninomiya. But it was also assumed higher for quartz in band 13 than band 12 as it was assumed in QRI image. Therefore, quartz enrichment in granite and alkali granite was delineated using QI–RH index as it was done in QRI image (Fig. 5.a and c). In FRI image, feldspar enriched alkali granite was brighter than darker granitic patch as alkali granite was relatively rich in alkali feldspar (Fig. 5.d) We, however, found satisfactory performance of MRI and NMI index images in delineating mafic mineral impoverishment in granite and alkali granite exposures than weathered residuum developed above granodiorite gneiss; which was mafic rich (Fig. 5.e and f).While comparing Ninomiya's index images (NQI and NMI both) with the proposed QRI and MRI index images based on index values, we found relatively poor correlation between QRI and NQI while MRI and MFI was highly correlated (Fig. 6.a and b). Therefore, It indicated that MRI and NMI were complementary to each other. This observation can be used as self validation on the efficiency of MRI image in mafic mineral mapping as it was comparable with established NMI. But QRI was not comparable with NQI as it could better delineate silica enrichments in alkali granite than NQI. However, QRI was comparable with QI–RH in terms of delineating granitoids with higher quartz content. Therefore, regression analysis of two indices derived high correlation coefficient (Fig. 6.c). We also made a false colour composite using QRI, FRI and MRI indices to delineate different granitoids (Fig. 7). We could find that quartz enrichment of alkali granite was enhanced in Fig. 7 (FCC derived using new indices proposed in this study). It was delineated with “yellow” colour in RGB colour display as index values of QRI and FRI were higher for alkali granite due to its enrichment with both quartz and feldspar. In this image, granite exposures are pinkish red in colour and granodiorite gneiss exposures are bluish green (in surface, it is covered with green coloured soil cover) (Fig. 7).We also derived three dimensional scatter-plot using proposed three index values to delineate three major sub-variants of granitoids from each other (Fig. 8). It was observed that three variants of granitoids can be separated from each other in QRI–FRI–MRI data space. Exposures identified as granite, alkali

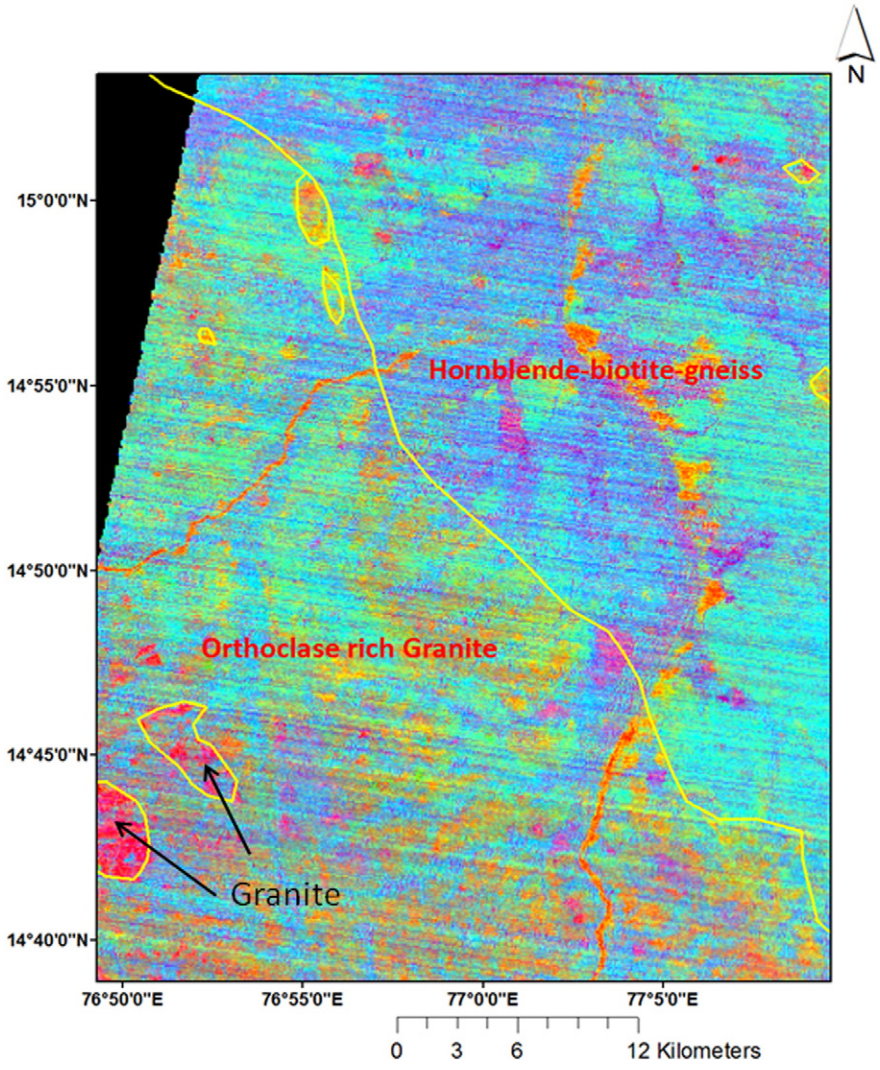

Fig. 7. False colour composite (FCC) derived using QRI-FRI-MRI indices to delineate feldspar poor part of granite from alkali granite and hornblende-biotite granodioritic gneiss.

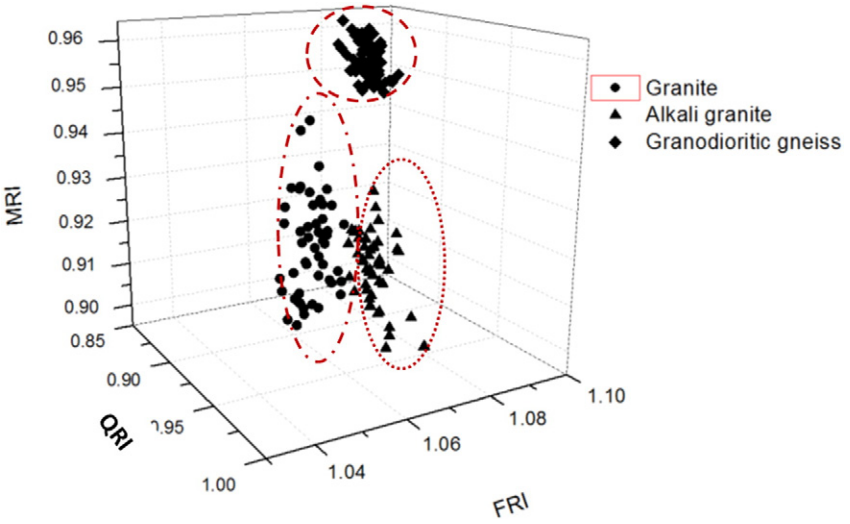

Fig. 8. 3-dimensional scatter plot used to differentiate alkali granite- granite and hornblende-biotite-granodioritic gneiss in QRI–MRI–FRI plot.

granite and granodiorite-gneiss using in these index images and their combination (Figs. 5.a.c and 7) were validated spectrally by comparing their respective image-derived emissivity spectra with the laboratory counter part of ASTER resampled emissivity spectra of similar rocks (Fig. 9.a and b).We find image-derived emissivity spectra and laboratory counterpart of two major granitoid variants match well with each other as their spectra were comparable in terms of highlighting major emissivity minima of these rocks. Spectral library of rocks of John Hopkins Laboratory (this library is available with ENVI 4.8 software) was used as reference in this case (JHU, 2015)

We also attempted to understand the relation between proposed index values (based on the comparison of selected index pairs) to test them in terms of mineralogical framework of granitoids. In this regard, we analysed the regression plots of index values with combinations of QRI and MRI, MRI and FRI, QRI and FRI for granite–alkali granite–granodiorite exposures to understand the efficiency of these indices in delineating gradual variations in mineralogy of granitoids and conceptually testing them based on proven pattern of mineralogical variations observed in granitoids (Fig. 10.a.b.c). We found that the QRI and MRI indices were inversely proportional to each other (regression value 0.85).

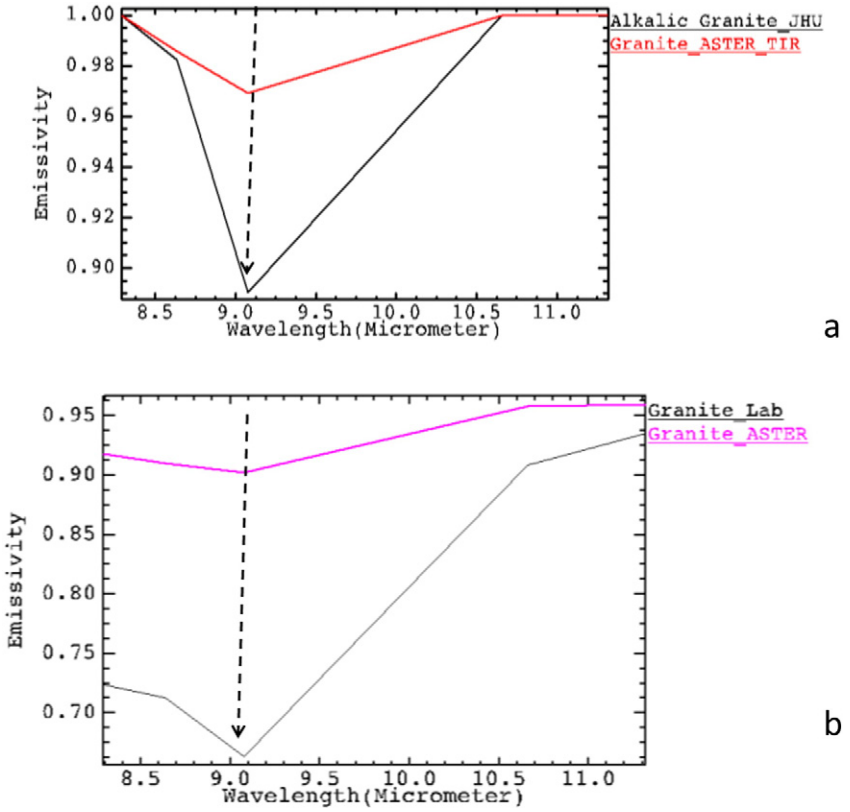

Fig. 9. a. Comparison between ASTER TIR band resampled laboratory spectra of alkali-granite with image spectra of rock exposures delineated based on using QRI–FRI–MRI composite. b. Comparison between ASTER TIR band resampled laboratory emissivity spectra of granitoid with image derived emissivity spectra of rocks exposures; which were identified in QRI–FRI–MRI composite. Emissivity image was derived using emissivity normalisation method (emissivity minima are shown with arrow).

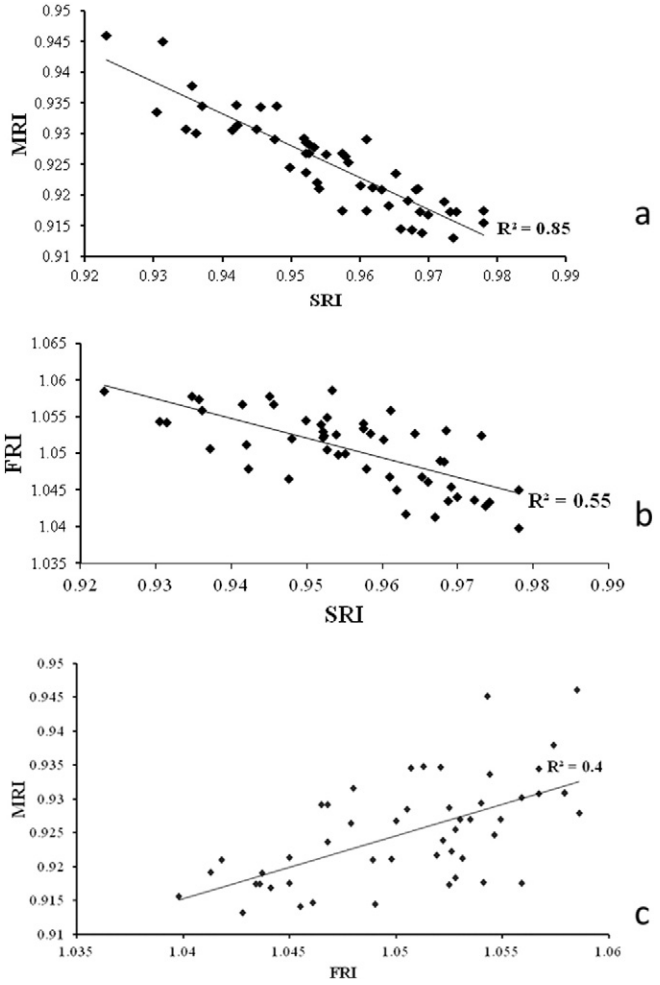

Fig. 10. a. Correlation between QRI and MRI. b. Correlation between QRI and FRI. c. Correlation between MRI v/s FRI.

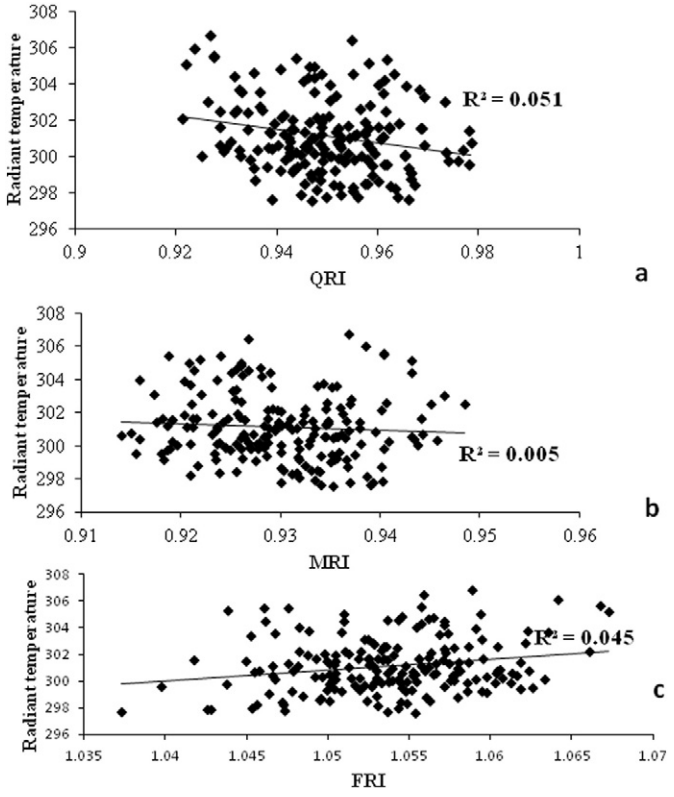

Fig. 11. a. Correlation between relative surface temperatures with QRI. b. Correlation between relative surface temperatures with QRI. c. Correlation between relative surface temperatures with MRI.

This was in congruence with basic mineralogical framework of inverse relation between mafic and quartz mineral abundances in granitoids (Fig. 10.a).On the other hand, FRI and QRI had poor negative correlation (0.55) as feldspar content (plagioclase feldspar) of granitoids would increase with the gradual decrease in quartz content in general in the sequence of granite–granodiorite–tonalite (Fig. 10.b).However, alkali feldspar content was often high in quartz-rich granite but alkali feldspar abundances in this granite may also increase with or without the increment of feldspar. The factors mentioned above, contributed in negative correlation between QRI and FRI with low regression value. MRI and FRI were positively correlated with regression value 0.4 as feldspar content increases with the increase in mafic content in plagioclase feldspar rich granodiorite. However, mafic mineral content in K-feldspar rich granites is low in general (Bose, 1997) (Fig. 10.c).

We also tried to understand the sensitiveness of these three indices to surface temperature (Ding et al., 2014). Relative surface temperature image derived during emissivity and temperature separation using emissivity normalisation method was used as reference to understand the temperature influence on these indices. Potential of emissivity normalisation method and other relative emissivity extraction method in deriving surface temperature has been already discussed in the literature (Gangopadhyay et al., 2005; Payan and Royer, 2004; Li et al., 2013a). Rocks of the present study area are known for very similar thermal inertia as these rocks belong to the same intrusive rock family with similar thermal conductivity, specific heat and density. Therefore relative surface temperature image derived using emissivity normalisation method using ASTER data of the study area (collected under dry cold weather) was considered suitable to understand relative variation of surface temperature. We found poor correlations between three indices with temperature (Fig. 11.a.b.c). This indicated that the index values of the proposed three indices would not be affected by relative surface temperature variation and would be useful in mineralogical mapping irrespective of surface temperature condition of terrain elements.

5. Discussions and conclusions

We have derived indices (QRI, FRI, MRI) from ASTER level 1B "at-sensor radiance" images; which are in turn derived from day time ASTER level 1B radiance data. These indices have been derived from "at-sensor radiance" data as similar ASTER derived mineralogical indices were earlier derived from same data sets (Ninomiya et al., 2005; Rajendran et al., 2011a,b, Matar and Bamousa, 2013; Aboelkhair et al., 2010; Ding et al., 2014, 2015). Derived indices could delineate granite, granodioritic gneiss and alkali-granite from each other. These indices are important as it could delineate variation in the content of quartz, feldspar and mafic minerals in granitoids. QRI is more effective in mapping high quartz content in alkali granite exposures than NQI index as NQI (Fig. 5.a and b) is derived based on the assumption of higher emissivity for quartz in band 11 in comparison to band 12 of ASTER thermal sensor. But alkali feldspar and quartz are characterised with inverse emissivity response in band 11 and bad 12 of ASTER thermal sensor. Therefore, quartz indices proposed using these two bands would have limitations in delineating quartz enrichments in granitoids; which are also enriched with K feldspar. Therefore, implementation of NQI for delineating quartz rich alkali feldspar granite could not derive a desirable result. Another spectral index (QI–RH) involving band 11, band 12, band 10 and band 13 however, could derive quartz enrichment comparable to QRI index (Rockwall and Hofstra (2008)). It is also observed that

MRI provided comparable information with that of established NMI in delineating mafic mineral variations in granitoids (Fig. 5.e and f).The correlation between MRI and NMI is also very high (Fig. 6.b). This observation also indirectly validates the MRI index. But correlation between NQI and QRI is poor (Fig. 6.a). It is also observed that QRI and QIRH had higher correlations while delineating quartz enrichment in granite and alkali granite. This provided indirect validation QRI index (Fig. 6.c).

It is also observed that conjugate use of QRI, MRI and FRI has given an idea about variation in feldspar and quartz content in three main granitoids. This was essential to segregate one granitoid variant from the other as it has been effectively done in index composite and three dimensional data plot of three indices (Figs. 7 and 8). Ratio of alkali-feldspar (K–Na Feldspar) to plagioclase feldspar (Ca and Na bearing feldspar) gradually decreases from alkali granite to tonalite in alkali granite–granite–granodiorite–tonalite sequence. Therefore, alkali granite being rich in quartz and K-feldspar minerals appeared with yellow colour in FCC image when QRI, FRI and MRI index bands were loaded with red, green and blue colour in FCC display (Fig. 7).

We could also spectrally validate the results of index based delineation of granitoids by comparing image derived emissivity spectra of granite and alkali granite exposures (emissivity spectra were derived by geospatially tagging index images with emissivity image) with ASTER-TIR band resampled laboratory spectra of respective rocks (Fig. 9.a and b) in addition to cross-checking the results using reference geological maps (Prepared by Geological Survey of India, GSI). Further, results of regression analysis of these indices (QRI vs. MRI, FRI vs. MRI, QRI vs. MRI) are in accordance with the broad mineralogical framework of granitoids (Fig. 10.a.b.c). It is already discussed that FRI is not suitable to segregate two feldspar groups from each other as both feldspars have broad emissivity minima in band 11 of ASTER (alkali feldspar and plagioclase feldspar).Therefore correlation of FRI with QRI and MRI is the outcome of combined effect of independent relation of each feldspar (alkali and plagioclase) with quartz and mafic minerals (Fig. 10.b and c). Alkali feldspar is positively correlated with quartz but negatively correlated with mafic minerals. On the other hand, abundance of plagioclase feldspar in granitoid is inversely proportional with the abundance of quartz but directly proportional with mafic minerals (as mafic minerals progressively increase from granite to tonalite with increment of plagioclase feldspar and consequent reduction in abundance of K-feldspar). Therefore, relationship between FRI and MRI is governed by two inverse mineralogical relations of two feldspar groups with mafic mineral. Similarly relationship between QRI and FRI is governed by the same aspect (i.e. inverse relationship of abundance of alkali feldspar and plagioclase feldspar with quartz). FRI has poor positive correlation with MRI in the study area as the area was dominantly made up of plagioclase rich granite (Fig. 10.c). Similarly, QRI had poor negative correlation with FRI as plagioclase feldspar abundance increases with the reduction in quartz in granitoid (Fig. 10.b).However, relation between QRI and MRI is straight forward (negatively correlated with high correlation value) and it is in accordance with mineralogical framework of granitoid. This can also be regarded as the conceptual validation of QRI and MRI index as mafic mineral and quartz is mutually exclusive in granites. Proposed index images are also weakly correlated with surface temperature image derived using emissivity normalisation method. This indicates that the indices can be used in mineralogical mapping even if same targets are exposed with different surface temperatures. Therefore, the proposed indices may be used successfully to delineate different granitic intrusions of variable mineralogy and would be helpful in providing better understanding of different quartz-rich magmatic phases and their relation with green-schist rocks of the Archaean period. This also would help in relating compositional variations of granitoids with metallogeny.

Acknowledgements

The authors are grateful to the Director, NRSC and Deputy Director, RSA for their guidance and over all support. The authors are also grateful to the anonymous reviewers for their constructive comments for improving the manuscript. The authors are deeply indebted to the Editor-in- Chief of Ore Geology Review for making important editorial corrections.

References

Aboelkhair, H., Ninomiya, Y., Watanabe, Y., Sato, I., 2010. Processing and interpretation of ASTER TIR data for mapping of rare-metal-enriched albite granitoids in the Central Eastern Desert of Egypt. J. Afr. Earth Sci. 58, 141–151.

Abrams, M., 2000. The Advanced Spaceborne Thermal Emission and Reflection Radiometer (ASTER): data products for the high spatial resolution imager on NASA's Terra platform. Int. J. Remote Sens. 21 (5), 847–859.

Bertoldi, L., Massironi, M., Visona, D., Carosi, R., Montomoli, C., Gubert, F., et al., 2011. Mapping the Buraburi granite in the Himalaya of Western Nepal: remote sensing analysis in a collisional belt with vegetation cover and extreme variation of topography. Remote Sens. Environ. 115 (5), 1129–1144.

Bose, M.K., 1997. Igneous Petrology. World Press, Kolkata.

Chen, J., Wang, A.J., 2007. The pilot study on petrochemistry components mapping with ASTER thermal infrared remote sensing data. J. Remote Sens. 11, 601–608.

Clark, R.N., 2011. Spectroscopy of Rocks and Minerals, and Principles of Spectroscopy. USGS spectral laboratory (http://speclab.cr.usgs.gov/spectral-lib.html (accessed on 07–12-11)).

Ding, C., Liu, X., Liu, W., Liu, M., Li, Y., 2014. Mafic and ultramafic and quartz-rich rock indices deduced from ASTER thermal infrared data using a linear approximation to the Planck function. Ore Geol. Rev. 60, 161–173.

Ding, C., Xuqing, L., Xiangnan, L., Liting, Z., 2015. Quartzose–mafic spectral feature space model: a methodology for extracting felsic rocks with ASTER thermal infrared radiance data. Ore Geol. Rev. 66, 283–292.

Drury, S.A., Harris, N.B.W., Holt, R.W., Reeves-Smith, G.J., Wightman, R.T., 1984. Precambrian tectonics and crustal evolution in south India. J. Geol. 92, 3–20.

Farmer, V.C. (Ed.), 1974. The Infrared Spectra of Minerals, 4. Mineralogical Society, London, p. 539.

Gangopadhyay, P.K., Maathuis, B., Van Dijk, P., 2005. ASTER derived emissivity and coalfire related surface temperature anomaly: a case study in Wuda, north China. Int. J. Remote Sens. 26 (24), 5555–5571.

Gillespie, A.R., 1985. Lithologic mapping of silicate rocks using TIMS. Proceedings of the. Thermal Infrared Multispectral Scanner Data User's Workshop, Pasadena, CA, June 18–19, pp. 29–44.

Gomez, C.c., Delacourt, C., Allemand, P., Ledru, P., Wackerle, R., 2005. Using ASTER remote sensing data set for geological mapping, in Namibia. Phys. Chem. Earth A/B/C 30, 97–108.

Guha, A., Vinod Kumar, K., 2014. Potential of Thermal Emissivity for Mapping of Greenstone Rocks and Associated Granitoids of Hutti–Maski Schist Belt,Karnataka. The International Archives of the Photogrammetry, Remote Sensing and Spatial Information Sciences, Hyderabad, India, pp. 423–430.

Guha, A., Vinod Kumar, K., 2015. Integrated approach of using aster derived emissivity and radiant temperature for delineating different granitoids — a case study in parts of Dharwar Craton, India. Geocarto Int. http://dx.doi.org/10.1080/10106049.2015.108690 (in press).

Guha, A., Rao, A., Ravi, S., Vinod Kumar, K., Dhananjaya Rao, E.N., 2012. Analysis of the potentials of kimberlite rock spectra as spectral end member — a case study using kimberlite rock spectra from the Narayanpet Kimberlite Field (NKF), Andhrapradesh. Curr. Sci. 103, 1096–1104.

Guha, A., Ravi, S., Ananth Rao, D., Vinod Kumar, K., Dhanamjaya Rao, E.N., 2013a. Issues and limitations of broad band remote sensing of kimberlite—a case example from kimberlites of Dharwar Craton, India. Int. J. Geosci. 4371–4,379.

Guha, A., Singh, V.K., Parveen, R., Vinod Kumar, K., Jeyaseelan, A.T., Dhanamjaya Rao, E.N., 2013b. Analysis of ASTER data for mapping bauxite rich pockets within high altitude. lateritic bauxite, Jharkhand, India. Int. J. Appl. Earth Obs. Geoinf. 21, 184–194.

Guha, A., Vinod Kumar, K., Dhananjaya Rao, E.N., Parveen, R., 2014. An image processing approach for converging ASTER derived spectral maps for limestone mapping-a case example for Kolhan limestones, Jharkhand, India. Curr. Sci. 106, 40–49.

Gupta, R.P., 2003. Remote Sensing Geology. Springer-verlag, p. 655.

Hook, S.J., Gabell, A.R., Green, A.A., Kealy, P.S., 1992. A comparison of techniques for extracting emissivity information from thermal infrared data for geologic studies. Remote Sens. Environ. 42, 123–135.

Hook, S.I., Abbott, E.A., Grove, C., Kahle, A.B., Palluconi, F., 1999. Use of multispectral thermal nfrared data in geological studies. In: Rencz, A.N. (Ed.), Manual of Remote Sensing, Third edition volume-3. John Willey and Sons, p. 699.

ITT, 2014. ENVI:(Thermal Data Pre-processing. http://www.exelisvis.com/portals/0/pdfs/envi/Flaash_Module.pdf2009 (accessed on 12–10-2014).

JHU, 2015. Johns Hopkins University Spectral Library. http://speclib.jpl.nasa.gov/documents/jhu_desc (accessed on 09.07.15)).

Kahle, A.B., 1976. Thermal inertia imaging: a new geologic mapping tool. Geophys. Res. Lett. 3, 419–421.

Kalinowski, A., Oliver, S.A., 2004. ASTER Mineral Index Processing Manual. http://www.ga.gov.au/image_cache/GA7833.pdf.

Kealy, P.S., Hook, S.J., 1993. Separating temperature and emissivity in thermal infrared multispectral scanner data: implications for recovering land surface temperatures. IEEE Trans. Geosci. Remote Sens. 31 (6), 1155–1164.

Li, Z.-L., Becker, F., Stoll, M.P., Wan, Z.M., 1999. Evaluation of six methods for extracting relative emissivity spectra from thermal infrared images. Remote Sens. Environ. 69, 197–214.

Li, Z.L., Tang, B.H., Wu, H., Ren, H., Yan, G., Wan, Z., Trigo, I.F., Sobrino, J.A., 2013a. Satellite derived land surface temperature: current status and perspectives. Remote Sens. Environ. 131, 14–37.
Li, Z.-L., Wu, H., Wang, N., Qiu, S., Sobrino, J.A., Wan, Z., Tang, B.-H., Yan, G., 2013b. Land surface emissivity retrieval from satellite data. Int. J. Remote Sens. 3084–3127.
Lyon, R.J.P., 1972. Infrared spectral emittance in geological mapping: airborne spectrometer data from Pisgah Crater. Science 7, 983–986.
Matar, S.S., Bamousa, A.O., 2013. Integration of the ASTER thermal infra-red bands imageries with geological map of Jabal Al Hasir area, Asir Terrane, the Arabian Shield. J. Taibah Univ. Sci. 7 (1), 1–7.
Murthy, M.R., Ramam, P.K., 1997. Geology of Andhra Pradesh. Geological Society of India, Bangalore.
Nair, A., Mathew, G., 2012. Lithological discrimination of the Phenaimata felsic–mafic complex, Gujarat, India, using the Advanced Spaceborne Thermal Emission and Reflection Radiometer (ASTER). Int. J. Remote Sens. 33, 189–219.
Ninomiya, Y., et al., 1997. A comparison of thermal infrared emissivity spectra measured in situ, in the laboratory, and derived from thermal infrared multispectral scanner (TIMS) data in Cuprite, Nevada, U.S.A. Int. J. Remote Sens. 18 (7), 1571–1581.
Ninomiya, Y., Fu, B., Cudahy, T.J., 2005. Detecting lithology with Advanced Spaceborne Thermal Emission and Reflection Radiometer (ASTER) multispectral thermal infrared radiance-at-sensor data. Remote Sens. Environ. 99, 127–139.
Okada, K., Iwashita, A., 1992. Hyper-multispectral IMAGE ANALYSIS BASED ON WAVEFORM. characteristics of spectral curve. Adv. Space Res. 12, 433–442.
Payan, V., Royer, A., 2004. Analysis of Temperature Emissivity Separation (TES) algorithm. applicability and sensitivity. Int. J. Remote Sens. 25, 15–37.
Peres, L.F., DaCamara, C.C., 2004. Land surface temperature and emissivity estimation based on the two-temperature method: sensitivity analysis using simulated MSG/SEVIRI data. Remote Sens. Environ. 91, 377–389.
Rajendran, S., Nasir, S., 2014. ASTER spectral sensitivity of carbonate rocks — study in Sultanate of Oman. Adv. Space Res. 53, 656–673.
Rajendran, S., Hersi, O.S., Al-Harthy, A., Al-Wardi, M., El-Ghali, M.A., Al-Abri, A.H., 2011a. Capability of Advanced Spaceborne Thermal Emission and Reflection Radiometer (ASTER) on discrimination of carbonates and associated rocks and mineral identification of eastern mountain region (Saih Hatat window) of Sultanate of Oman. Carbonates Evaporites 26, 351–364.
Rajendran, S., Thirunavukkarasu, A., Balamurugan, G., Shankar, K., 2011b. Discrimination of iron ore deposits of granulite terrain of Southern Peninsular India using ASTER data. J. Asian Earth Sci. 41, 99–106.
Rockwall, B.W., Hofstra, A.H., 2008. Identification of quartz and carbonate minerals across northern Nevada using ASTER thermal infrared emissivity data-Implications for geologic mapping and mineral resource investigations in well-studied and frontier areas. Geosphere. 4, 218–246.
Rowan, L.C., Mars, J.C., Simpson, C.J., 2005. Lithologic mapping of the Mordor, NT, Australia ultramafic complex by using the Advanced Spaceborne Thermal Emission and Reflection Radiometer (ASTER). Remote Sens. Environ. 99 (1–2), 105–126.
Salisbury, J.W.S., D'Aria, D.M., 1992. Emissivity of terrestrial materials in the 8–14 μm atmospheric windows. Remote Sens. Environ. 42, 83–106.
Salisbury, J.W., Walter, L.S., 1989. Thermal infrared (2.5–13.5 μm) spectroscopic remote sensing of igneous rock types on particulate planetary surfaces. J. Geophys. Res. 94 (B7), 9192–9202.
Sial, A.N., Bettencourt, J.S., De Campo, C.P., Ferreira, V.D., 2011. Granite-related ore deposits: an Introduction. Geol. Soc. Lond., Spec. Publ. 350, 1–5.
Son, Y.-S., Kang, M.-K., Yoon, W.-J., 2014. Lithological and mineralogical survey of the Oyu Tolgoi region, South-eastern Gobi, Mongolia using ASTER reflectance and emissivity data. Int. J. Appl. Earth Obs. Geoinf. 26, 205–216.
van der Meer, F.D., de Jong, S.M., Bakker, W., 2006. Imaging spectrometry: basic analytical techniques. In: Van der Meer, F.D., De Jong, S.M. (Eds.), Imaging Spectrometry: Basic Principles and Prospective Applications. Springer, Dordrecht, pp. 17–61.
van der Meer, F.D., et al., 2012. Multi- and hyperspectral geologic remote sensing: a review. Int. J. Appl. Earth Obs. Geoinf. 14, 112–128.
Yajima, T., 2014. ASTER Data Analysis applied to Mineral Resource Exploration and Geological Mapping (Ph.D thesis) Department of Earth and Environmental Sciences, Graduate School of Environmental Studies, Nagoya University.
Yajima, T., Yamaguchi, Y., 2013. Geological mapping of the Francistown area in northeastern Botswana by surface temperature and spectral emissivity information derived from Advanced Space-borne Thermal Emission and Reflection Radiometer (ASTER) thermal infrared data. Ore Geol. Rev. 53, 134–144.
Zhang, X., Pazner, M., Duke, N., 2007. Lithologic and mineral information extraction for gold exploration using ASTER data in the south Chocolate Mountains (California). ISPRS J. Photogramm. 62, 271–282.